

Scientific report – extended summary

January – December 2018

Open problems in radiological risk assessment of tritium emissions including climate changes PN-III-P4-ID-PCE-2016-0218 – IDEI 191/2017 (OPTRAS)

The radiological risk assessment of tritium transfer into the environment involves tritium concentration in feedstuffs/foodstuffs after their processing and storage and highly depends on the dynamics of tritiated water (HTO) and organically bound tritium (OBT) concentration in plant compartments many weeks before harvest. For HTO transfer, the balance between air to plants and soil to plants pathways must be better understood. OBT production in plants involves complex biochemical processes and depends on the dynamics of HTO concentration in leaves. The upgrades of a dynamic operational model for tritium transfer (as HTO and OBT) in crops (CROPTRIT) together with model tests and validation with the available experimental data for winter wheat was presented in the Report for 2017. The selected crops are specific to Cernavoda NPP site (Romania) operating two CANDU 6 reactors where winter wheat is of first concern, then pasture, maize, and wine grapes (order of planting). The full data base of Romanian agricultural research was accessed. Night processes involved in OBT production are considered in the upgraded CROPTRIT model. In the present report, CROPTRIT adaptation to pasture is presented together with other activities.

For CROPTRIT adaptation to grass, the main task was to develop the sub-growth model according to grass physiology and to change accordingly the physiological parameters, taking into account the mowing. Mowing induces changes in the model, because part of the OBT is lost, but part of it, still remains in the plant. The growth sub-model considers the effects of genotype (phenology, new dry matter partition), management (fertilisation, irrigation) and weather on the pollutant concentration at harvest. The crop growth sub-model includes the vertical nitrogen distribution in grass and is based on a simplification regarding the dependence of nitrogen content in leaves on the development stage and fertilization. The model is run with different time steps for meteorological data, starting with 10 minutes up to one hour for plant physiological parameters. A reserve compartment was added as a sink before flowering and as a source afterwards. Respiration has a slow component (mostly due to protein turnover) and a separated compartment was added. Starch (insoluble) is accumulated at day and is degraded (hydrolysed) after sunset in soluble forms in order to assure leaf respiration, protein turnover and export, avoiding carbon shortage.

As for the dry matter production, the maintenance and growth respiration are considered in order to assess the net production of OBT, which thereafter is distributed to the grass parts. The difference between agricultural models and the present plant growth sub-model is the time step (1 day versus 10 minutes up to 1 hour). Generally, the agricultural models use a time step of a day, but the present plant sub-growth model uses a time step of 10 minutes up to one hour and consequently, this short time step affects the assessment of gross assimilation in photosynthesis, respiration and the plant development stage (DVS), respectively. The main difficulty resides in the non-linear dynamics of temperature during the day time. Excepting GECROS model (Yin and van Laar, 2005), all the plant growth models uses an average of minimum and maximum temperature during the day time for both respiration and photosynthesis. In CROPTRIT model, hourly temperature is used and differences between hourly and daily assimilation and respiration, respectively are noticed (Fig. 1).

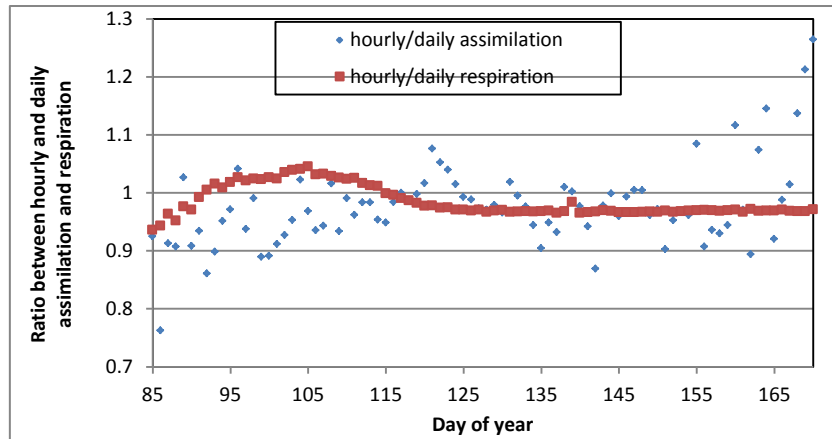


Fig. 1. The ratio between hourly and daily assimilation and respiration calculated with an hourly time step

For grass, the evapotranspiration was modelled based on a dual source approach, which makes the distinction between the grass canopy and soil, as well as between the grass transpiration and soil evaporation. The dual source model (Shuttleworth and Wallace, 1989) was adapted for tritium (Melintescu and Galeriu, 2005) and assumes the knowledge of the net radiation and that absorbed by soil and consequently, the equations for various fluxes and conductances are more complicated. Atmospheric, boundary layer and soil resistances were changed accordingly to grass characteristics. Grass/pasture is not that tall (about 50 cm) as other crops and consequently, the atmospheric and boundary layer resistances are lower, but they cannot be neglected. Root depth for grass is about 0.2 m and the exchange velocity between air and soil is strongly influenced by the soil resistance. In order to parameterise the soil resistance, the experimental data of Kondo et al. (1990, 1992, 1994, 1997) were analysed and the following relationship for soil resistance was obtained:

$$R=R_{\min}+R_{\max}\exp\{A[(\theta/\theta_{fc}-B)/(C-B)]^2\}$$

where: θ – fraction of volumetric water content in the first 2 cm of soil cm; θ_{fc} – soil field capacity; R_{\min} – minimum soil resistance, constant for all soil types ($= 10 \text{ s m}^{-1}$); R_{\max} – maximum soil resistance with the following values: 3000 s m^{-1} for sand; 2000 s m^{-1} for clay; 1500 s m^{-1} for loamy clay and volcanic ash; A, B, C – constants indicating the soil irregularities and the clay content soil, with the following values: $A=-7$, constant for all soil types; $B=0.11$ (sand); 0.074 (loamy clay); 0.03 (clay, sandy clay, thin sand); 0.06 (volcanic ash); $C = 1.3$ (sand); 0.95 (loamy clay); 0.75 (clay, sandy clay, thin sand); 0.63 (volcanic ash).

Based on the previous parameterization, the model reproduces the experimental data from Kondo et al. (1990, 1992, 1994, 1997) with a factor less than 2 for loamy clay, clay and alluvial sand and the independent data sets are reproduced by the soil sub-model with a factor 3 (Fig. 2).

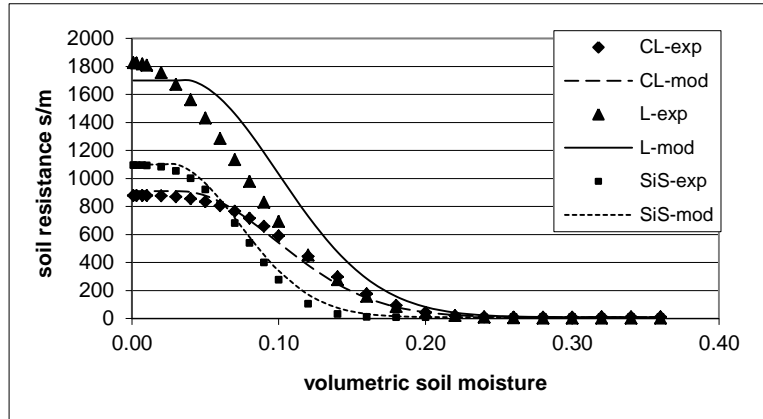


Fig. 2. Comparison between model results and experimental data for soil resistance

The model results for HTO concentration in grass for two values of leaf area index (LAI) and for dry and wet soil, is given in Fig. 3. In Fig. 3, it is noticed that the coupling between soil surface and grass has a significant influence on canopy resistance. For both high and low values of LAI and for wet soil, the HTO concentration in grass is significantly higher than for dry soil for the same values of LAI.

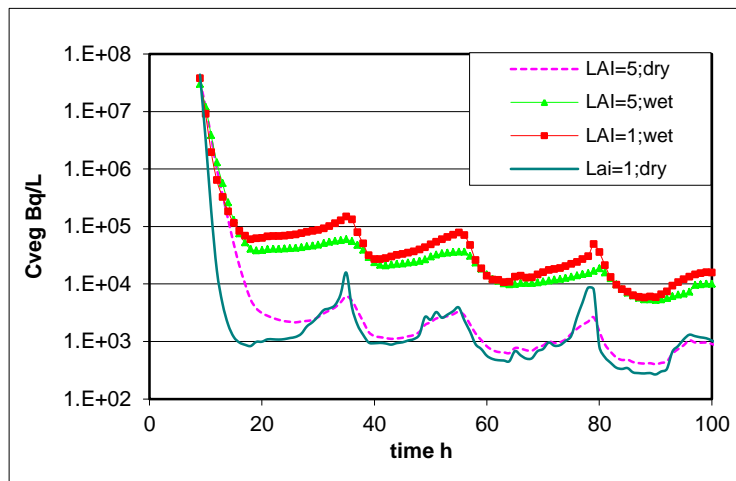


Fig. 3. HTO concentration in grass

For OBT production in grass, the same formalism as for wheat was used (Galeriu and Melintescu, 2017), but taking into account that grass is cut at every two months. The assimilate initially produced in photosynthesis is a soluble sugar having the glucose structure. Part of the assimilate is converted partially in sucrose and partially is exported. Grass produces starch which during the night time is hydrolysed in soluble forms and used for grass respiration and export. At morning, the sucrose is accumulated from the new assimilate and at night from starch. The adjustment of sucrose and starch metabolism is to ensure a balanced export at day and night. CROPTRIT model considers that starch degradation (hydrolysis) and the assimilate allocation between sucrose and starch is controlled by a daily integral of carbon assimilation on photosynthesis duration. The changing of allocation ratio does not induce a different export, but a changing between day and night exports.

For CROPTRIT application to grass, the detailed physiological processes were considered including the protein turnover. We demonstrated that protein turnover can explain the OBT formation and persistence in leaves/grass, even after the stop of grass growth or cutting and has a delay effect of its transfer to the new growing grass after cutting. CROPTRIT model is based on the dynamics of proteins and non-structural carbohydrates from grass and the OBT production is based on water addition reaction of HTO (Galeriu and Melintescu, 2017; Melintescu et al., 2015).

Based on these theoretical assumptions, CROPTRIT model was applied for grass (and other plants from Cernavoda area), considering an emission of 11 PBq (30 g) of HTO for an hour, atmospheric stability class F, emission at 50 m distance, wind speed of 1 m/s on plume direction – the worst case scenario. The model results are given in Figs. 4 (HTO) and 5 (OBT). It is noticed the abrupt decreasing of HTO concentration (Fig. 3) after the plume passage, to values of 100 times lower than for the cases when the plume is on. The OBT concentration (Fig. 5) strongly increases in the first 10 hours, it has a slower increase the next day after the plume passage and stays constant up to hour 70.

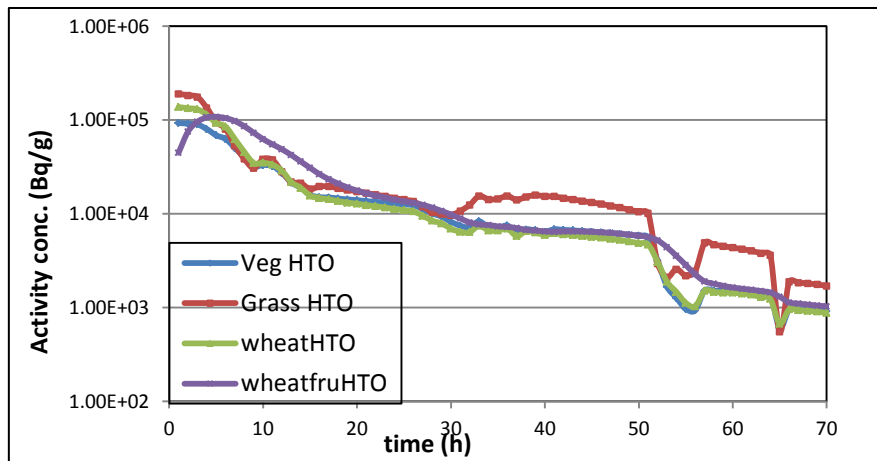


Fig. 4. HTO concentration in grass, wheat and vegetables leaves and wheat grain

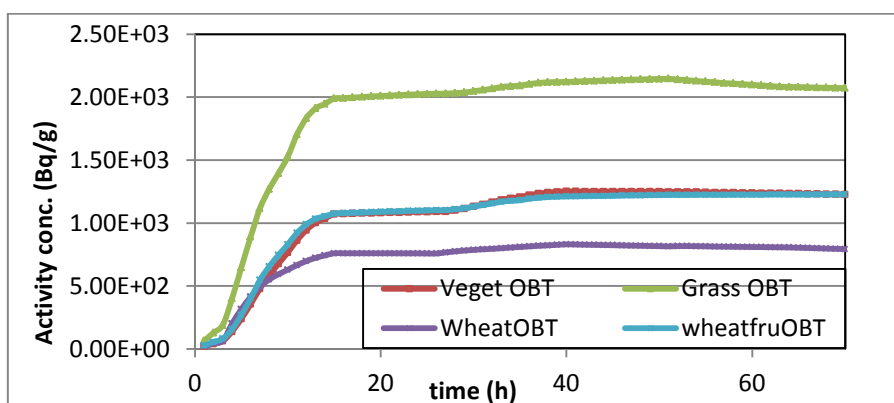


Fig. 5. OBT concentration in grass, wheat and vegetables leaves and wheat grain

The adaptation of CROPTRIT model to grass demonstrates that the model being based on the detailed analysis of plants physiology, is versatile and able to estimate the HTO and OBT concentration in grass (and other plants) in case of an accidental/incidental emission of tritium at Cernavoda NPP. Unfortunately, the experimental data are sparse.

Another activity for the Scientific Report in 2018 was the NUCLEAR Meteorology, because tritium transfer in plants is strongly correlated with the meteorological parameters, in order to achieve the meteorological data base and the understanding of correlations between meteorological factors and the tritium transfer in agricultural plants. Consequently, efforts have been done to properly operate the Met Tower of IFIN-HH. We equipped the Met Tower with a new laser source for the ceilometer (providing information about the cloud cover necessary for the estimation of solar radiation scheme used in CROPTRIT model) and a novel measurement configuration according to the novel requirements for nuclear meteorology. The new configuration, as the previous one, assures the data acquisition of the meteorological parameters in real-time on-line as 10 minutes averages of the parameters registered at 10 seconds, as it is asked for the radiological emergency.

Based on the meteorological system, we analysed the meteorological data regarding the temperature gradient, net solar radiation, standard deviation of wind direction, wind speed at 30 and 60 m, and the correlations between all these parameters (Fig. 6) and we estimated the flux of sensible heat at soil surface and the solar height. Based on these correlations and observations, we developed a specific procedure and we developed the meteorological and radiological data base of IFIN-HH. For 2015-2017 periods, the meteorological data base covers 95 % for the whole time period and the statistical analysis of the data provides the distribution of atmospheric stability classes for the all 16 sectors of wind direction (Fig. 7). The meteorological system of IFIN-HH works automatically un-attended and provides on-line data at 10 minutes for local emergency system. The new configuration system is still tested, in order to provide quality assurance meteorological and radiological data.

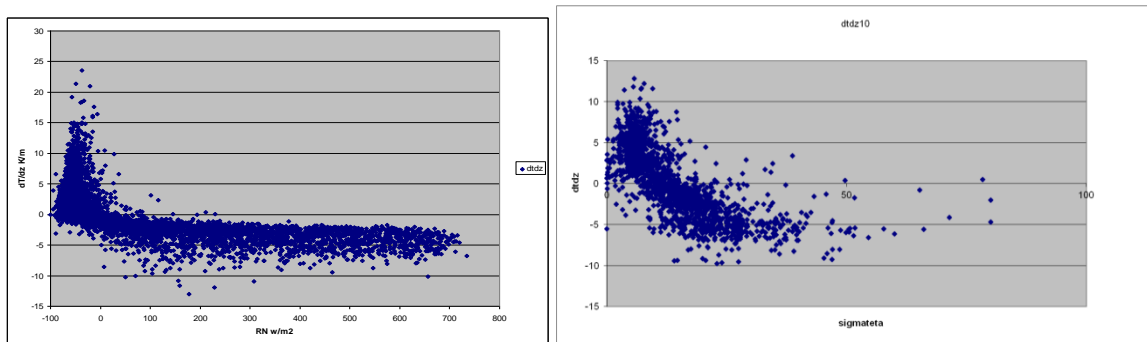


Fig. 6. Correlation between thermal gradient and net radiation (left) or standard deviation of wind direction (right)

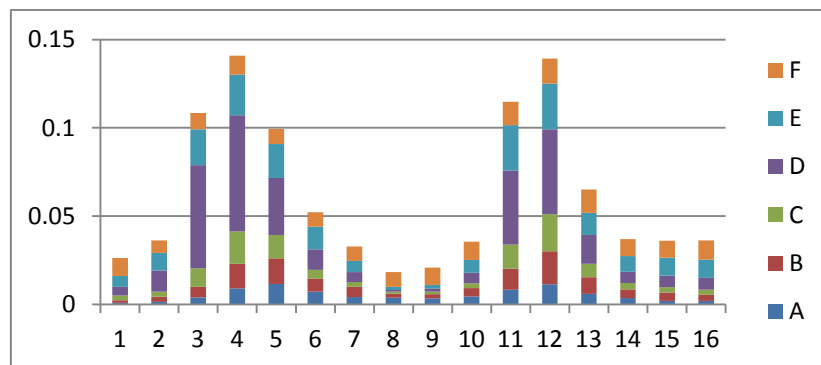


Fig. 7. Statistics of atmospheric stability classes at IFIN-HH. Class A – unstable, D – neuter, F – stable. Sector 1 represents North.

The results obtained with the previous configuration of the Met Tower for 2015-2018 are in accordance with the requirements of the nuclear meteorology, but efforts must be done in future, in order to have quality assured meteorological data provided by the new configuration.

Another important activity this year was the influence of radon on ambient gamma dose rate and the correlation with precipitations. Radiological emergencies at nuclear facilities (e.g. Chernobyl in 1986; Fukushima in 2011) as well as unregulated or regulated weapons testing or detonations, have the potential to spread hazardous radioactive fallout over extensive regions of the. Mitigation of the potential health effects from such incidents relies heavily upon early identification of the threat, and a rapid response. Since gamma-emitting radionuclides are common to most forms of nuclear-related fallout, near-surface monitoring of the “ambient equivalent gamma radiation dose rate” has become widely adopted as a means of identifying such events. Continuous monitoring of the near-surface ambient gamma dose is performed routinely at major nuclear facilities, but also more generally on the country level at various locations around Europe. This monitoring network constitutes the main component of a country-level early warning system for radiological emergencies. The sensitivity and efficacy of this country-level warning system depends upon (i) the quality of observations (instrument performance and consistency of quality control/analysis procedures), and (ii) the level of understanding of the variability in the near-surface ambient gamma dose due to other contributing factors.

Natural factors contributing to the spatial and temporal variability in the near-surface ambient gamma dose include: cosmic radiation, local soil and rock characteristics (natural radionuclides in the soil), soil water content, atmospheric concentrations of short-lived naturally-occurring gamma emitting aerosols (e.g. progeny of ^{222}Rn and ^{220}Rn) that can change with atmospheric stability, and precipitation (snow or rain) that can concentrate gamma emitting aerosols at the surface (Bossey et al., 2017; Barbosa et al., 2017; Levin and Cotton, 2008). In the absence of nuclear events, each monitoring station of the network provides useful information about background levels of the ambient gamma dose, which is site specific. Observations from each station can then be analysed to characterise the local terrestrial component of the ambient gamma dose and its natural variability (e.g. as a predictor of geogenic radon potential) (Bossey et al., 2017), information that is subsequently used to derive indicator thresholds for nuclear incidents. However, before reliable thresholds or indicators can be developed for radiological emergencies it is necessary to understand the natural short-term variability in ambient gamma dose resulting from meteorological factors that might otherwise be misinterpreted as an incident/event. The majority of data reported from all local or national European ambient gamma dose monitoring stations are non-validated, implying that anomalies associated with changing meteorological conditions (including periods of atmospheric stability or heavy precipitation), and malfunctions of the equipment hardware or software, have not been identified and removed, so they can appear as erroneous high values. Consequently, isolated activity-threshold-alarms in these datasets cannot automatically be treated as a true indication of a dangerous increase in levels of radioactivity. Since significant ambient gamma dose variability can result from natural causes, this limits the current ability to generate prompt alerts of potential malfunctions of nuclear facilities or other external nuclear accident.

The IFIN-HH is situated in a suburban area of southern Romania (44°21'2.72"N, 26°02'38.42"E), about 10 km southwest of the Bucharest central business district. The atmospheric monitoring system at IFIN-HH utilises a 60m meteorological tower. Continuous measurements of wind speed, wind direction, temperature and relative humidity are made at 30 and 60m above ground level (a.g.l.). Net radiation, solar radiation and rainfall are monitored at 30m a.g.l., atmospheric radon concentration at 10m a.g.l. (or 2m from 2015),

and the ambient gamma dose is monitored at 1.5m a.g.l. (or 2m from 2015). In the immediate vicinity of the site, within the measurement fetch, there is a heterogeneous mix of trees and buildings that vary in height from 10 to 15 m a.g.l. All observations from the monitoring system are logged as 10-min averages of 10-s readings and subsequently integrated to hourly averages for analysis. In addition to the meteorological observations already described by Galeriu et al. (2011, 2014), atmospheric radon concentration is monitored using an “AlphaGUARD” (PQ2000 PRO, Saphymo, Germany; which also separately monitors atmospheric pressure, temperature and relative humidity). As described in Chambers et al. (2016), the AlphaGUARD was situated in a Stevenson's Screen (well-ventilated, weatherproof enclosure) to protect it from precipitation, operated in diffusion mode, and set for hourly integration. The ambient gamma dose is measured using a GAMMATRACER (XL2-2- RS232).

When the short-lived ^{222}Rn progeny ^{214}Pb and ^{214}Bi are deposited on the ground by rain, they significantly increase the near-surface (above ground) ambient gamma dose. Within a short period of time the rainwater containing ^{214}Pb and ^{214}Bi can migrate into the soil and form a volume source. For a short, low-intensity, rainfall event the contaminated soil layer is thin, and the depth of penetration depends on the initial soil water content. For a prolonged rainfall event, contaminated water from the start of the event is pushed deeper into the soil, resulting in a radioactivity profile with a quasi-exponential shape. The simple IFIN-HH model assumes that in-cloud processes take sufficient time to ensure that secular equilibrium between radon and its progeny has been attained at cloud base. Water loss rate from cloud is also considered to be related to the rainfall rate, and the progeny concentration of rain drops at cloud base is dependent on the total quantity of water in the cloud. At the soil surface, the progeny flux depends on the cloud base-to-ground transport time, over which the radioactive chain disintegrations occur. Precipitation rate and the diameter distribution of rain drops also play important roles. For simplification, the IFIN-HH model assumes the average diameter of raindrops to be function of the precipitation rate. It also uses a relaxation depth (α) of about 0.5, which is acceptable for a prolonged rainfall event. Further details regarding the model formulation are provided in Galeriu (2015).

All meteorological, atmospheric radon, and ambient gamma dose observations from the IFIN-HH meteorological tower site between 2010 and 2016 were quality checked and processed. Due to budgetary and staffing constraints equipment maintenance was challenging. Over this 7-year period, the times when all instrumentation (meteorology at all heights, solar and net radiation, radon concentration and ambient gamma dose) were operating simultaneously often occurred in stretches of only several months at a time. Consequently, where discussion relies upon the availability of all (or most) datasets, specific time periods have been selected for analysis, typically from the years 2011-12 and 2015-16. The most continuous year of ambient gamma dose observations was 2012, so this year has been chosen to describe seasonality. In 2012 the seasonal cycle of monthly-mean terrestrial background ambient gamma dose at IFIN-HH was characterised by maximum values (101–102 nSv h⁻¹) between July–October, when there are extended periods of relatively little precipitation (Fig. 8c), and a pronounced minimum in February (about 75 nSv h⁻¹; see also Fig. 8a), at the time of maximum snow cover. “Excess gamma” is defined here as the difference between what is observed hourly as the ambient gamma dose and our estimate of the terrestrial background gamma radiation. This difference is usually the result of increases in the ambient gamma dose due to rain events or changes in the near-surface radon concentration. On a monthly average basis, Fig. 8b and c indicate a reasonable correlation between months of higher rainfall and months of higher excess gamma dose. However, the relationship between these two parameters is clearly not consistent throughout the year. In the winter months some of the non-correlation between precipitation and higher excess gamma dose is likely attributable to

excess gamma dose occurring as a result of snowfall that is not accurately recorded by the rain gauge at 30m on the IFIN-HH tower. However, another contributing factor to excess gamma is the build-up of radon and radon progeny near the ground under stable nocturnal atmospheric conditions.

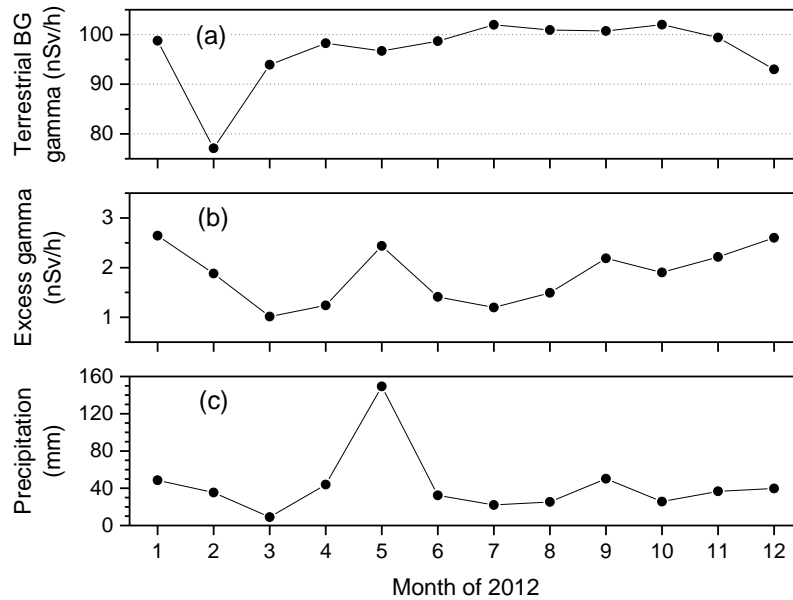


Fig. 8. Monthly mean hourly (a) observed ambient gamma dose, (b) excess gamma, and (c) precipitation

Excluding rainfall influences, the second most significant factor contributing to short-term (diurnal to synoptic timescales) variability in the ambient gamma dose is changes in near-surface concentrations of atmospheric radon. Typically the largest variability in near-surface radon concentration at a site occurs on diurnal timescales as a result of changes in atmospheric mixing. Since radon is a noble short-lived radioactive gas, with a relatively consistent uniquely-terrestrial source, near-surface changes in radon concentration are closely related to changes in the atmospheric mixing state (Chambers et al., 2011; Williams et al., 2013). As described by Chambers et al. (2015, 2016) and Williams et al. (2016), average values of the near-surface radon concentration over a nocturnal window (e.g. 2000–0500 h) can be used to assign atmospheric “stability categories” to whole nights of extended datasets (> 3 months). During the autumn of 2011 nightly observations from the IFIN-HH tower were classified as occurring under one of three atmospheric mixing categories: well-mixed, moderately-mixed or stable. As shown in Fig. 9a, when nocturnal conditions were well-mixed there was only a relatively small-amplitude diurnal cycle of radon concentration observed at 10m a.g.l. Conversely, for stable nocturnal conditions the average amplitude of the diurnal radon cycle was around 35 Bq m^{-3} (standard deviation $\pm 11 \text{ Bq m}^{-3}$). For rain-free well-mixed conditions (Fig. 9b) there was very little diurnal cycle evident in the ambient gamma dose. Conversely, when stable nocturnal conditions prevailed there was an average diurnal amplitude of around 6 nSv h^{-1} in the ambient gamma dose signal measured at 1.5m a.g.l. Barbosa et al. (2017) also reported an influence of atmospheric stability on the near-surface gamma dose.

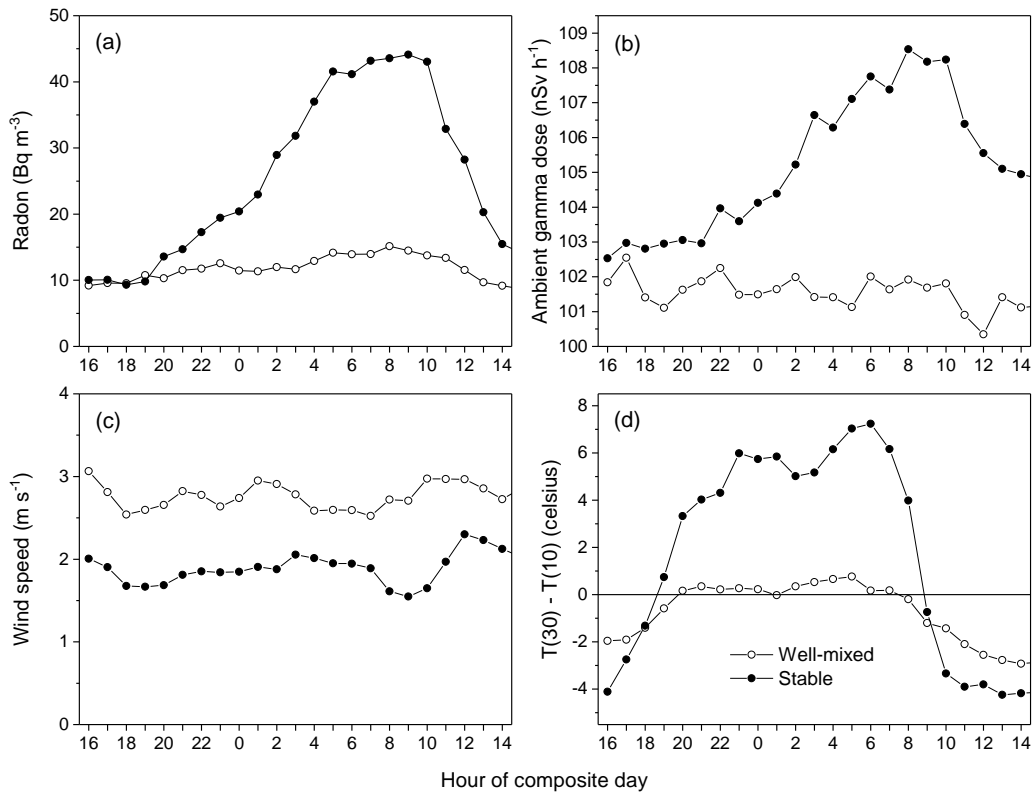


Fig. 9. Diurnal composite radon concentration, wind speed and ambient gamma dose under well-mixed and stable nocturnal atmospheric mixing conditions at IFIN-HH in autumn 2011

When ambient gamma dose and precipitation records were analysed, correlations were observed between the excess gamma dose and precipitation events. At times, the excess gamma dose was 60–80% above the seasonal terrestrial background signal. Peaks closely corresponded to the onset of precipitation events, but frequently lasted some hours after the precipitation had ceased. Gamma dose excess values of up to 70% over terrestrial background were also observed for some periods in 2016 (Fig. 10a). Again, these events corresponded well with precipitation events (Fig. 10b).

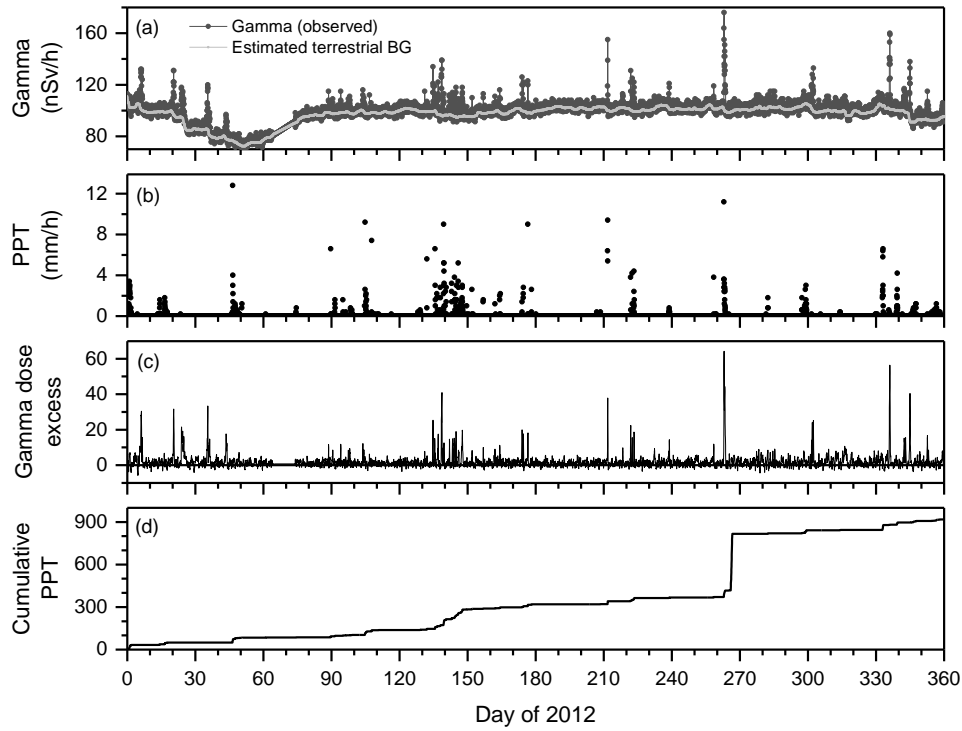


Fig. 10. Relationship between ambient gamma dose, precipitation and ^{222}Rn concentration

The simple IFIN-HH model performs well in simulating the excess gamma dose associated with this event (Fig. 11, 12). Initially the model under-estimates the observations, but is then comparable to, or slightly greater than, observed values. In all cases, differences between simulated and observed values are less than a factor of 2. The good performance of the simple IFIN-HH model in this case demonstrates that a good balance has been achieved with the model formulation. While there is still scope for the IFIN-HH model code to be upgraded, its current performance is already quite good.

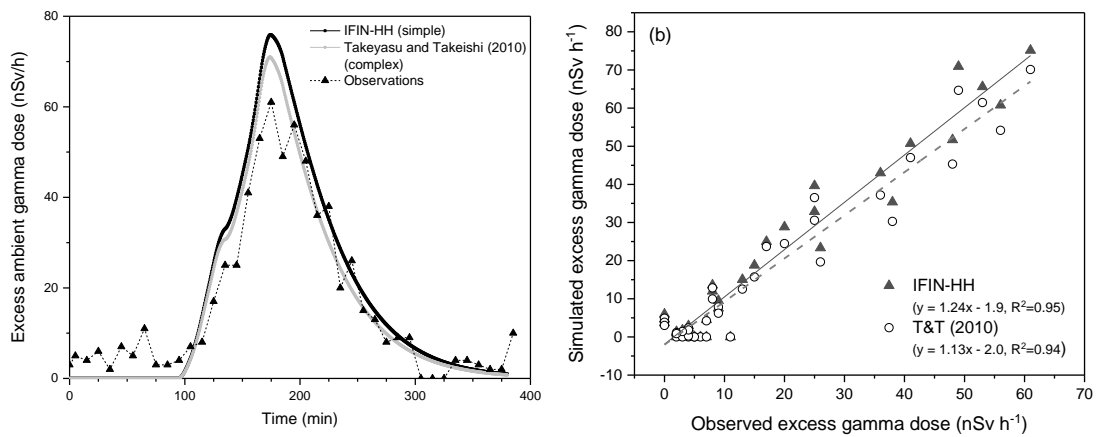


Fig. 11. Comparison between experimental excess of gamma dose rate and predictions of a simple (IFIN-HH model) and a complex model (Takeyasu and Takeishi, 2010) (June 2, 2015)

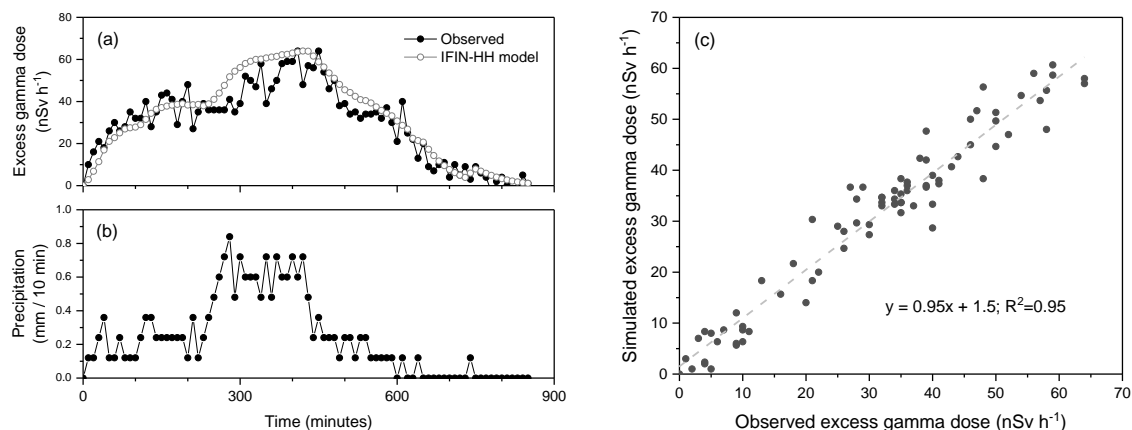


Fig. 12. Observed and simulated ambient gamma dose at IFIN-HH for a rainfall event on 2–3 December 2012, overlain with scaled 10-min precipitation

The simple model of this study is demonstrated to perform equally well or better than published models of higher complexity (e.g. Takeyasu and Takeishi, 2010). Simulated excess gamma dose (net signal after background removal) compared well with observed values. In cases when the simulations underestimated observations the magnitude of the difference was typically less than that of the variability in ambient gamma dose arising diurnally from atmospheric mixing effects (which are typically $< 15\%$ of the background ambient gamma dose). Consequently, by a combination of the automatic event detection method and removal of simulated rainfall influences on ambient gamma dose using a simple model, it should eventually be possible to reduce the present real-time attention limits for potential radiological incidents from 200 to 400% above background levels to 25–50% in near real-time. However, further refinement of the model used in this study is recommended, as is improvement to the consistency of data quality, and access to supplementary data (including cloud height, depth, and synoptic situation) is highly desirable.

Another topics of the present report was the interception and uptake by plants leaves of tritium from precipitation, pointed out as an important topics, unsolved by IAEA (IAEA, 2014). In the absence of experimental data for leaf HTO concentration due to tritiated rain, the present study considers various processes of potential importance such as: leaf interception during rain event, maximum water storage capacity of crops, leaf - water processes, interaction between drops and leaf surface, and extension of water layer (adhesion fraction). Recent results on pesticide spray experiments and modelling approaches (Gaskin et al., 2005; Merer et al., 2007; Forster et al., 2012, 2013; Massinon et al., 2012, 2014; Boukhalfa and Massinon, 2014; Dorr et al., 2014, 2016; Yao et al., 2014)) are used, because they provide useful information for the interaction between water droplet and leaf surface. The present study is focused on the main crops (*i.e.* wheat, maize, barley, soybean, oilseed rape, and grape) around Cernavoda Nuclear Power Plant (NPP) (Romania), operating two CANDU 6 units with high tritium loads. Cernavoda area has relatively low precipitations (lower than 500 mm y^{-1}) and the majority of precipitation events have intensities lower than 1 mm h^{-1} (Busuioc et al., 2012). In the last three years, climate changes on global scale have also influenced the local precipitation pattern (Busuioc et al., 2012). On a yearly scale, fewer precipitations were observed, but short periods of very high rain intensity after a dry season were registered in adjacent areas (Busuioc et al., 2012). Consequently, for radiological impact assessment of tritium, the present study tries to clarify the importance of tritiated rain on crops at harvest for normal and/or short term and intense tritium release.

The present study is based on information regarding sprinkler irrigation and pesticide spray (Gaskin et al., 2005; Merer et al., 2007; Forster et al., 2012, 2013; Massinon et al., 2012, 2014; Boukhalfa and Massinon, 2014; Dorr et al., 2014, 2016; Yao et al., 2014), in order to assess the processes occurred during a tritiated rain event and consequently, it is needed to point out the difference regarding the drop diameters distribution and falling velocity. The rain drop diameters distribution and the associated drop falling velocity are linked with the washout studies and past results for tritium are used (Belovodksi et al., 1997; Belot, 1998; Patryl and Armand, 2002; Golubev et al., 2002; Golubev et al. 2003; Guetat and Patryl, 2008; IAEA, 2008; Atanassov and Galeriu, 2011; Patryl et al., 2011; IAEA, 2014).

Canopy interception represents the amount of precipitation remaining on the leaf surface of the plant after the rain fall and entering the plant through the stem flow (Dunne and Leopold, 1978) and depends strongly on:

(1) vegetation type and stage of development, which can be characterized by the leaf area index (LAI);

(2) intensity, duration, and frequency of rainfall or irrigation.

A first successful theoretical approach was previously provided (Beard, 1976) and thereafter confirmed by modelling approaches (van Boxel, 1997; Khvorostyanov and Curry, 2002). For practical purposes, simple relationships (Mätzler, 2002 and the present study) are used:

$$\begin{array}{ll}
 V_T = 0. & D < 0.03 \text{ mm} \\
 V_T = 4.323 * (D - 0.03) & 0.03 < D < 0.6 \text{ mm} \\
 V_T = 9.65 - 10.3 * \exp(-0.6 * D) & D > 0.6 \text{ mm}
 \end{array}$$

Where: V_T is the terminal velocity of rain drop (m s^{-1}); D is the drop diameter (mm).

Based on the simple relationships given in equation (9) and various experimental data (Gunn and Kinzer, 1949; Best, 1950; Kessler, 1969; Foote and du Toit, 1969; Atlas and Ulbrich, 1973; Atlas et al., 1977; Uplinger, 1977; Willis, 1984; Brandes et al., 2002; Andronache, 2004; Loosmore and Cederwall, 2004), the terminal rain drop velocity for diameters between 0.1 and 1 mm are given in Fig. 13 and those for diameters between 1 and 6 mm are given in Fig. 14.

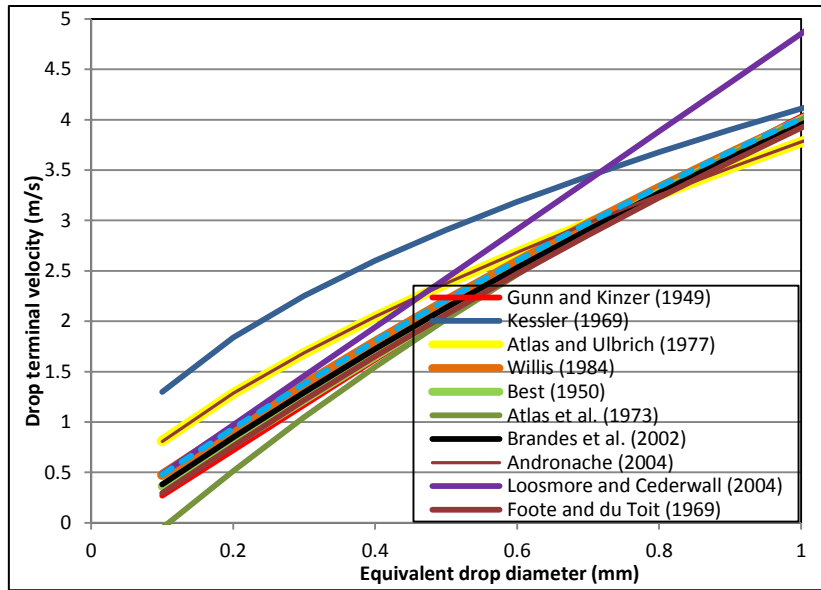


Fig. 13. Terminal rain drop velocity for the range of drop diameter between 0.1 – 1 mm

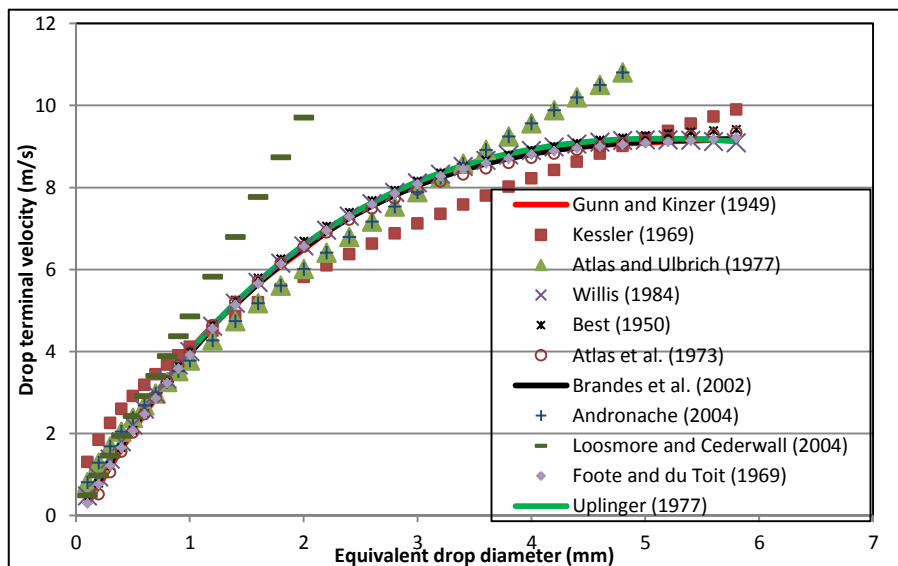


Fig. 14. Terminal rain drop velocity for the range of drop diameter between 1 – 6 mm

The drop size distribution (DSD) for some typical rain intensities is given in Fig. 15. All drops contained in a volume of height V_T fall on soil in one second. Considering a bin size of 0.1 mm for the drop diameter, the number of drops falling per m^2 in a second is given in Fig. 16, where it can be observed that the contribution of drops with diameters larger than 1 mm increases with the rain intensity. Those large drops are expected to splash initially on the leaves and to adhere only on leaves at the bottom of the canopy. At low rain intensity the contribution of small drops is high and it is expected a higher adhesion. In pesticide spray, drop diameters are lower than 1 mm and in case of rain, the fraction of drops falling with diameters lower than 1 mm varies with rain intensity. For the majority of rain events near CANDU reactors in Romania, drops with diameters lower than 1 mm prevails and the

experimental data on pesticide spray can be applied directly. Only for heavy rain, the splashing drops must be followed in their subsequent history.

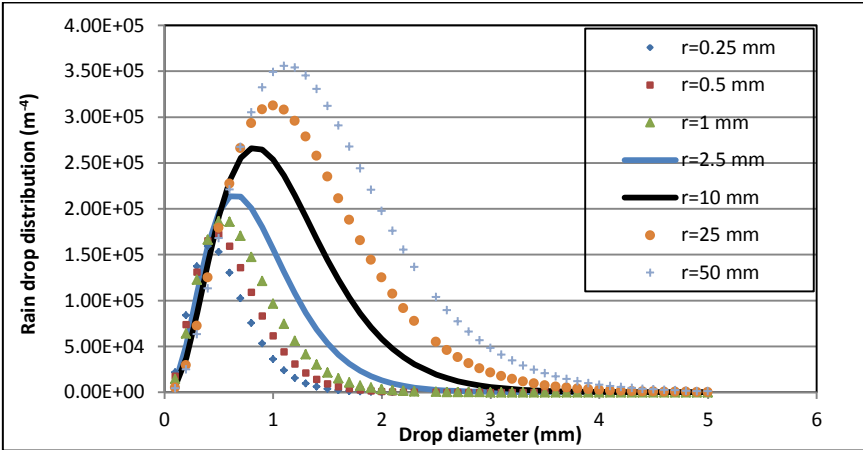


Fig. 15. Drop size distribution density per m^4

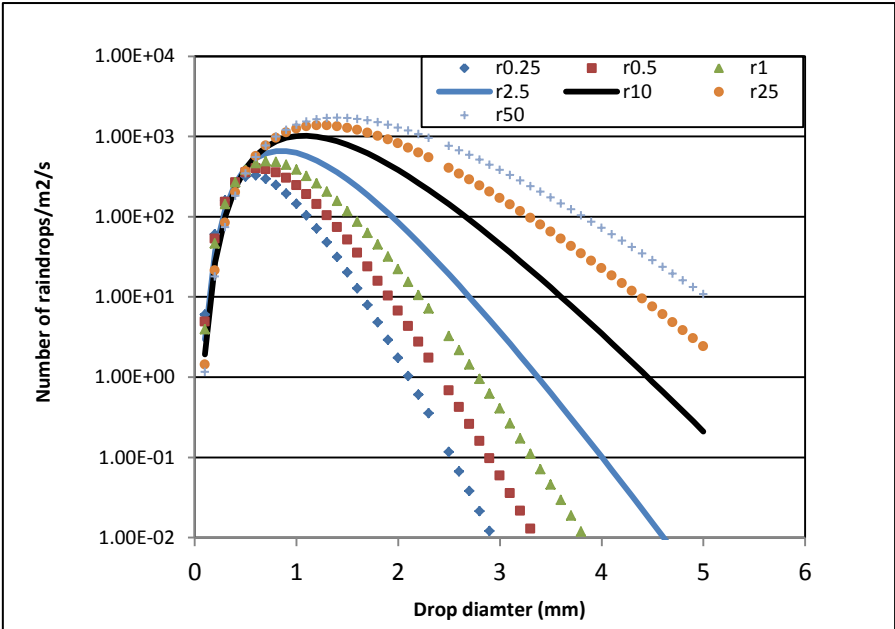


Fig. 16. Numbers of drops falling per m^2 in a second considering a bin size of 0.1 mm for the drop diameter

The adhesion of spray drop on wheat leaves was analysed for various impact velocities and diameters (Fig. 17).

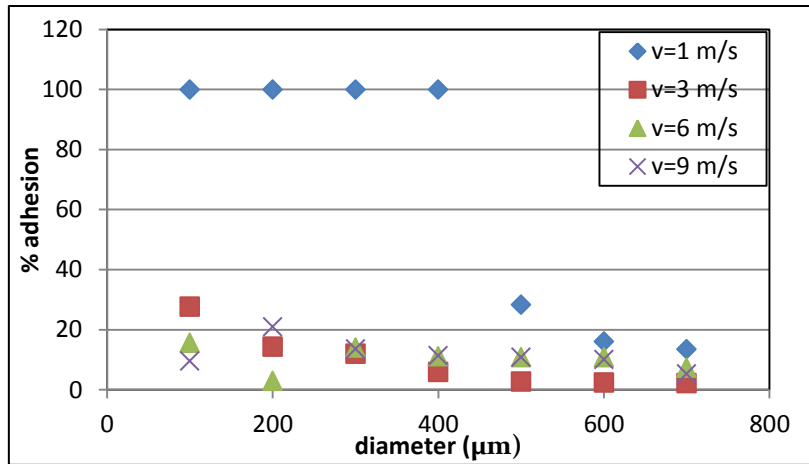


Fig. 17. Adhesion of spray drops for various impact velocities and diameters

For wheat, the results are given in the Fig. 18. The link between drop diameter and terminal velocity (D_{rain}) is compared with the border for bounce (D_{ad}) and shatter (D_{shat}). It is clear that only small drops adhere at the initial impact.

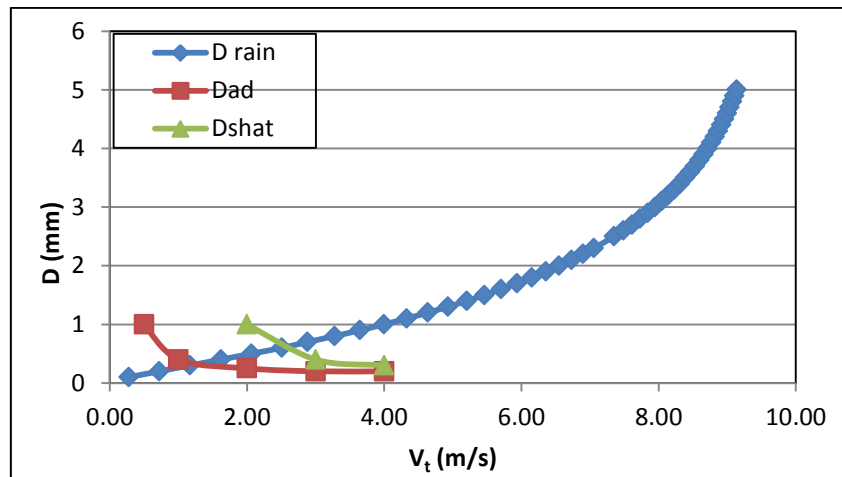


Fig. 18. Drop diameter and boundary of bounce and shattering regime for various falling velocities

The previous results are valid also for barley, maize, soybean, oil seed rape and cabbage. For grape, based on Nairn approach (Nairn et al, 2014), the adhesion is higher than for wheat. For dry bean, in the initial impact, drops with diameter lower than 1 mm adhere, the adhesion is higher than for wheat and grape and the stomata are covered with water after one hour of rain.

As a preliminary conclusion, the rain duration and wettability of crop are important factors affecting the leaf HTO concentration during the rain event. For difficult to wet crops, the stomata are more in contact with the surrounding air than with the rain water.

All the activities declared for this year were accomplished and the present results will be used for the next milestones of the present project.